Https://doi.org/10.36377/1726-7242-2022-20-1-28-35
Check for updates
CC BY

Investigation of cyclic fatigue of rotary endodontic instruments

© Zurab S. Khabadze, Farukh R. Ismailov,
RUDN University, Moscow, Russia

Abstract:
Aim. To study the properties and resistance to cyclic loading of nickel-titanium files with a martensitic phase. The use of nickel-titanium instruments is an integral part of the endodontic treatment of root canals. During endodontic treatment, nickel-titanium instruments experience a huge load, which is manifested by fatigue of nickel-titanium instruments, in the form of a fracture.
Purpose. To determine the resistance of nickel-titanium files to mechanical, chemical and temperature stress.
Materials and methods. A nickel-titanium file with a martensitic S-flexi phase from Geosoft was selected as a study. Cyclic fatigue was determined using a simulation endodontic unit. Photo and video fixation was carried out as a calculation of the revolutions and breakage time of the tool in the process of determining cyclic fatigue. To assess changes in the structure of nickel-titanium instruments with a martensitic phase, electron scanning microscopy and determination of the elemental composition of the alloy were carried out.
Results. In the course of the study, tests were carried out to determine the cyclic load, close to the clinical reception. After a series of cyclic load detection tests, S-flexi files showed different resistance to cyclic load. The results of cyclic fatigue are summarized in Table 1.
Conclusion. High-quality and safe mechanical treatment of root canals is possible when using nickel-titanium S-flexi files. Due to the high resistance to mechanical, chemical and thermal stress.

Keywords: S-flexi files, cleanliness, remnant, retreatment; root canal.

Received: 18.01.2022; **revised:** 25.02.2022; **accepted:** 03.03.2022.

Conflict of interests: The authors declare no conflict of interests.

Acknowledgments: There are no funding and individual acknowledgments to declare.

For citation: Zurab S. Khabadze, Farukh R. Ismailov. Investigation of cyclic fatigue of rotary endodontic instruments. Endodontics today. 2022; 20(1):28-35. DOI: 10.36377/1726-7242-2022-20-1-28-35.

INTRODUCTION

With the help of Walia et al., in 1988, nitinol was introduced into endodontics [25]. The use of nickel-titanium files has become the gold standard for mechanical treatment of root canals, due to the superelasticity and shape memory [25]. Despite all the achievements, the problem of file breakage is still present in the treatment of root canals [21, 26].

The main causes of file breakage are: torsion load and cyclic fatigue. Torsion load is the moment of retention of one part of the tool in the root canal while the rest continues to rotate.

Cyclic loading is the fatigue destruction of metal that occurs when the tool rotates cyclically in a curved state. What simulates the effect of repeated flexion and extension?

Torsion load occurs when the machining protocol is violated and the manufacturer's recommendations are not followed. Considering these factors, it is possible to avoid the phenomenon of torsion load. With the right selection of tools and work according to the manufacturer's recommendations, it is possible to avoid tool breakage.

It is difficult to predict the moment of breakaway, due to the cyclic fatigue of the instrument [16, 19, 20, 22]. Based on this, studies have been conducted to study the mechanism that leads to the break-off of nickel-titanium instruments. To increase the resistance to breakage under cyclic load, there are various processing methods: mechanical, electropolishing, thermal and electric charging treatment. [10, 11, 17, 18, 23]. All these methods are aimed at changing the metallurgical composition and changing the characteristics of the alloy, which in turn is manifested by phenomenal flexibility, resistance to cyclic and torsion loads, high cutting capacity, resistance to the influence of acids and alkalis [7, 8, 24]. These acquired properties of the alloy reduce the likelihood of tool breakage during treatment [5, 6, 9]. But the probability of uncontrolled breakage will remain relevant. Nickel-titanium alloy is relatively bioinert, and in turn, does not initiate inflammation, but due to the preliminary obturation of the root canal with an endodontic instrument, the possibility of full-fledged mechanical and medical treatment and further three-dimensional obturation decreases. [27-30]. There are a huge number of methods for extracting a tool fragment from the root canal. Due to the fact that the fragment of the tool crashes and gets stuck in the root canal. All methods are aimed at releasing tissues around the fragment of the instrument, which can lead to: perforation, overheating of the periodontium, weakening of the root of the tooth, pushing the fragment into the periodontium, etc.

The aims of the study are following:

1. Determine the limit of resistance to cyclic loading of nickel-titanium files introduced into clinical reception.
2. Identify signs of breakage of nickel-titanium files with a martensitic phase.

MATERIALS AND METHIODS

A scientific and methodological analysis of the Russian and foreign databases of medical and biological publications was carried out. An objective method for determining cyclic fatigue of nickel-titanium instruments with a martensitic phase has not been found. The existing methods for determining cyclic fatigue are mainly calculated for nickel-titanium files

with an austenitic phase [1, 2, 3].To determine the cyclic fatigue of a nickel-titanium instrument with a martensitic phase, it was decided to use a simulation endodontic unit with the condition of repeating work in curved root canals at a clinical reception.

The simulation endodontic unit consists of 5 channels with different bends (90º, 45º, 30º, double bend 45º and triple bend 45º). The simulation endodontic unit has an organic glass cover. NSK Endo-Mate TC2 was used as an endomotor. S-FLEXI (ENDOLINE/GEOSOFT) files were selected as files with the martensitic phase. The mode of operation with the tools was set in accordance with the manufacturer's recommendations.

The process of determining cyclic fatigue.

For the cyclic fatigue test, which is close to the clinical reception, it was decided to carry out 3 stages of testing an endodontic file:

1. The S-Flexi instrument was used on a simulated endodontic device for vertical translational passive file insertion with a rotation of 38-40 seconds in each channel: SF20/04 (400 rpm/2.5 N.cm), SF25/04 (400 rpm/1.5 N.cm), SF30/04 (400 rpm/1.5 N.cm), SF35/04 (400 rpm/1.5 N.cm), SF25/06 (400 rpm/2.0 N.cm).
2. Chemical load test. It was carried out by immersing the file in 3.25% sodium hypochlorite for 2 hours. Then, the file was washed with water and again immersed in a disinfectant solution (5% luminol solution) for 45 minutes, which includes alkyldimethylbenzylammonium chloride (HOUR) and glyoxal, surfactant, dye and water.
3. Physical activity test. The packed endodontic instrument was subjected to thermal cycling – autoclaving under the influence of 134°C, 1.2 atm for 45 minutes. This was the end of the first cycle of a full-fledged cyclic fatigue test. The resistant file was subjected to a second load cycle after the first one.

In the process of mechanical loading, a video recording was made, for calculating the number of revolutions and seconds performed before the break.

For a detailed inspection of the structure of the nickel-titanium instrument, electron scanning microscopy and studies of the structure and elemental composition were carried out on a JEOL JSM-6480LW microscope from JEOL with an energy dispersive prefix (EDX) X-MAX from Oxford Instruments (detector area 80mm2). A comparative examination of nickel-titanium instruments on an electron scanning microscope before and after loading was carried out. The image pattern was obtained in secondary electrons (SEI) and in back-reflected electrons (WT).

RESULTS

The total operating time of the nickel-titanium instrument in the canal of the imitation endodontic block was calculated from the moment of the first turn to the moment of files failure. The number of revolutions was calculated on the condition that we work at a speed of 400 revolutions per minute. Therefore, we divide 400 revolutions by 60 seconds to understand how many revolutions the file produces per second. According to calculations, it turns out 6.67 revolutions per second. Then the number of revolutions is multiplied by the number of seconds until the moment of capture, and thus we get the number of revolutions before the break. The data obtained differ from the manufacturer 's recommendations.

The samples were sent for scanning microscopy for a detailed examination of the fracture boundary.

Scanning microscopy was carried out on a JEOL JSM-6480 LW microscope manufactured by DEAL with an energy dispersive prefix (EDX) X-MAX manufactured by Oxford Instruments (detector area 80mm2). The images were obtained in the secondary electrons in three different magnifications (300x, 1000x, 5000x) and in the back-reflected electrons also in three different magnifications (300x, 1000x, 5000x).

The fractograms of the split surface of the cross-section of the new unused S-flex 4.20 sample show a homogeneous finely dimpled structure (Fig. 1a circles) with pointed wedge-shaped edges (Fig. 1a. doted circles.) and cliff-like fragments of structural elements ranging in size from 1 microns to 5.5 microns. The images show isotropic pores (Fig. 1b.arrows) located in almost every structural element of the surface and evenly distributed over the surface of the sample cleavage. Pores are observed mainly in the central zones of structural elements in the center of the pits and have sizes from 400 nm to 2 microns. No cracks were found.

On the fractograms of the split of the cross-section of the S-flex 4.20 sample obtained as a result of a series of workloads (1 cycle) including a twist fracture (volumetric stretching), a finely dimpled structure (Fig. 2a. circles.) less homogeneous than in the new sample with flatter and crumpled edges of structural elements ranging in size from 1 to 4.5 microns (Fig. 2a doted circles.) is visible. The fractogram also shows spherical perforation including lighter elements. Isotropic pores are observed mainly in the central zones of structural elements and have sizes from 500 nm to 2 microns (Fig. 2b arrows) . The pores are represented in large numbers and are evenly distributed over the surface of the sample cleavage. Alloy conglomerates of various shapes

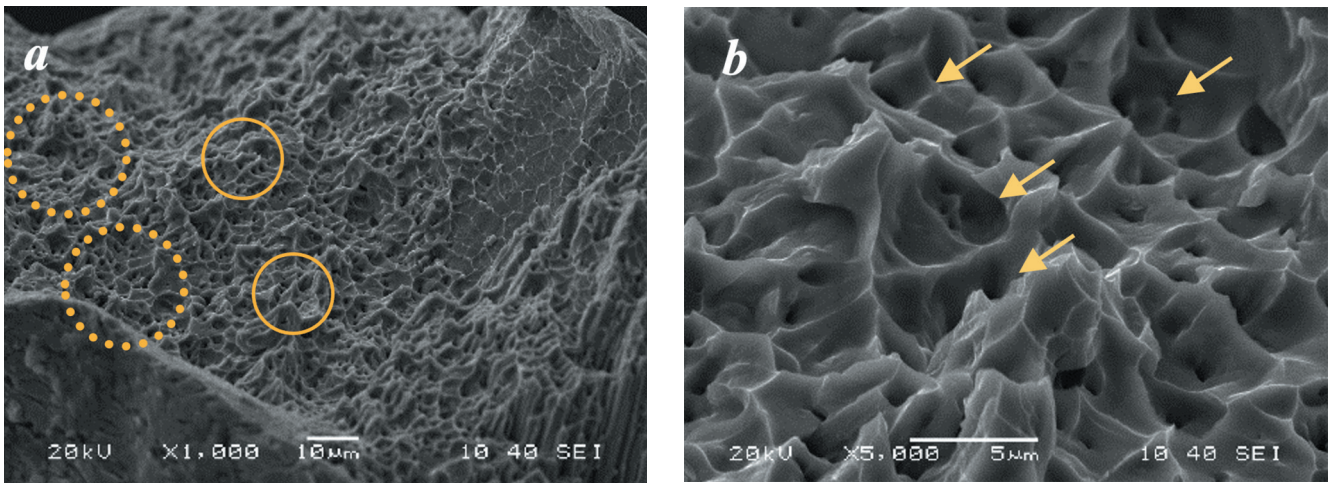

Fig. 1. **Fractograms of the split surface of a new, unused S-flex 4.20 sample-at different magnifications in secondary electrons.**

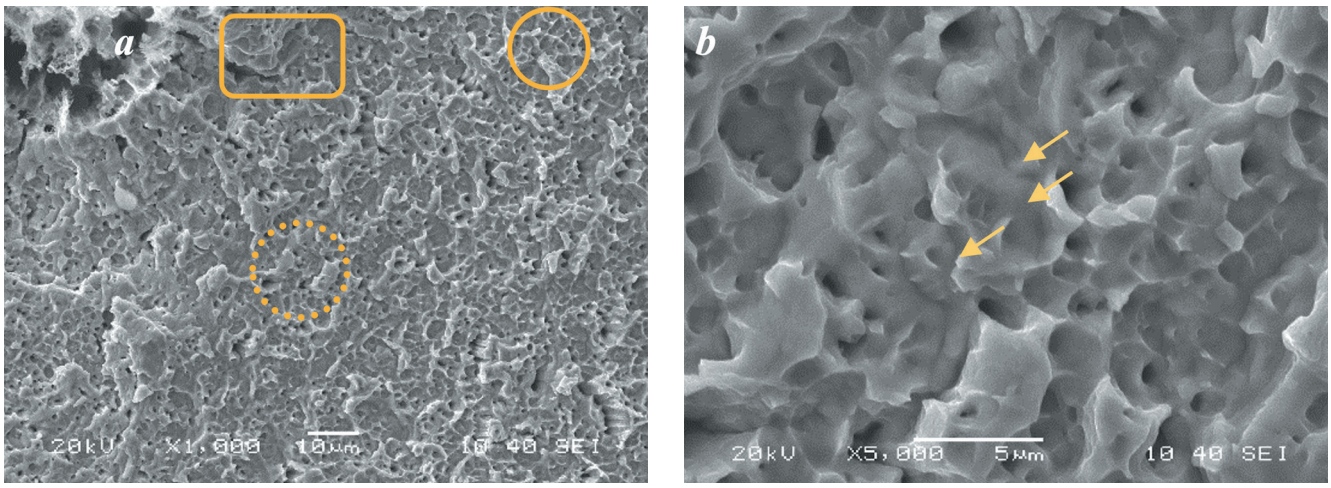

Fig. 2. **Fractograms of the split surface of the loaded, used S-flex 4.20 sample at different magnifications in secondary electrons.**

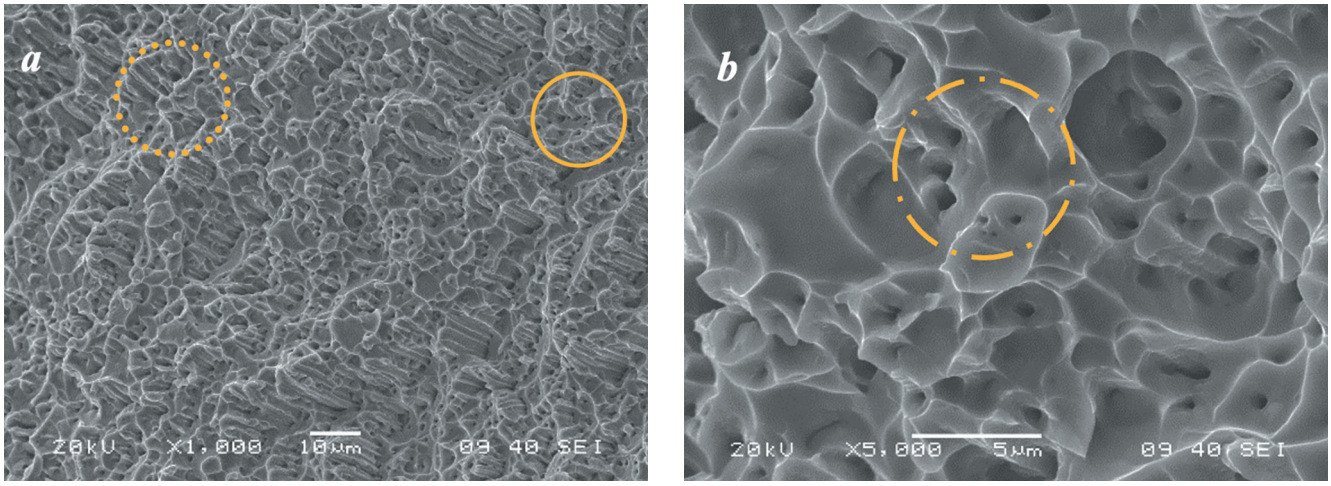

Fig. 3. **Fractograms of the split surface of a new, unused S-flex 4.25 sample at different magnifications in secondary electrons.**

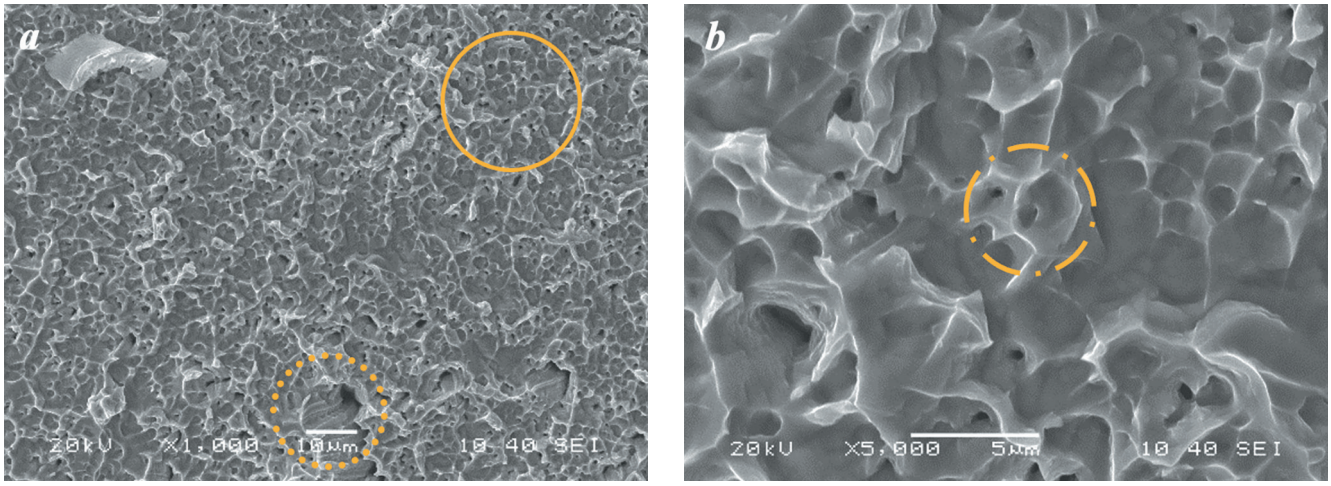

Fig. 4. **Fractograms of the split surface of the loaded, used S-flex 4.25 sample at different magnifications in secondary electrons.**

and sizes were found on the rock, which appeared during stretching and separation. In addition, cracks were found (Fig. 2 a squares) located in different parts of the sample and consisting of fused pores.

Fractograms of the split surface of a new, unused S-flex 4.25 sample at different magnifications in secondary electrons are demonstrated in Figure 3.

On the fractograms of the split of the cross-section of the S-flex 4.25 sample obtained as a result of a series of workloads (3 cycles), including a twist fracture (volumetric stretching), a finely dimpled structure (Fig. 4a circles) less homogeneous than in the new sample with flatter and crumpled wedge-shaped edges of structural elements with sizes from 1 microns to 5.5 microns is visible (Fig. 4b doted circle). Isotropic pores (Fig. 4b) are observed mainly in the central zones of structural elements and have sizes from 400 nm to 1 microns. The pores are observed in moderate amounts, in about half of the structural elements and are evenly distributed over the surface of the sample cleavage. Small conglomerates of alloy of various shapes and a crack consisting of fused pores (Fig. 4a circles and dotes) formed during stretching and separation were found on the rock.

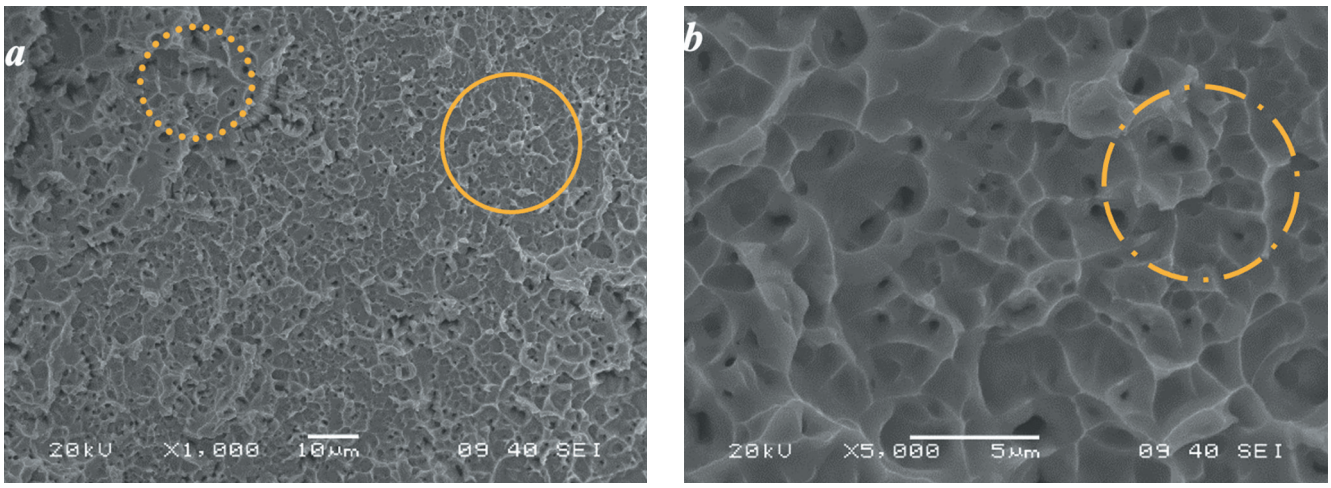

Fig. 5. **Fractograms of the split surface of a new, unused S-flex 6.25 sample at different magnifications in secondary electrons.**

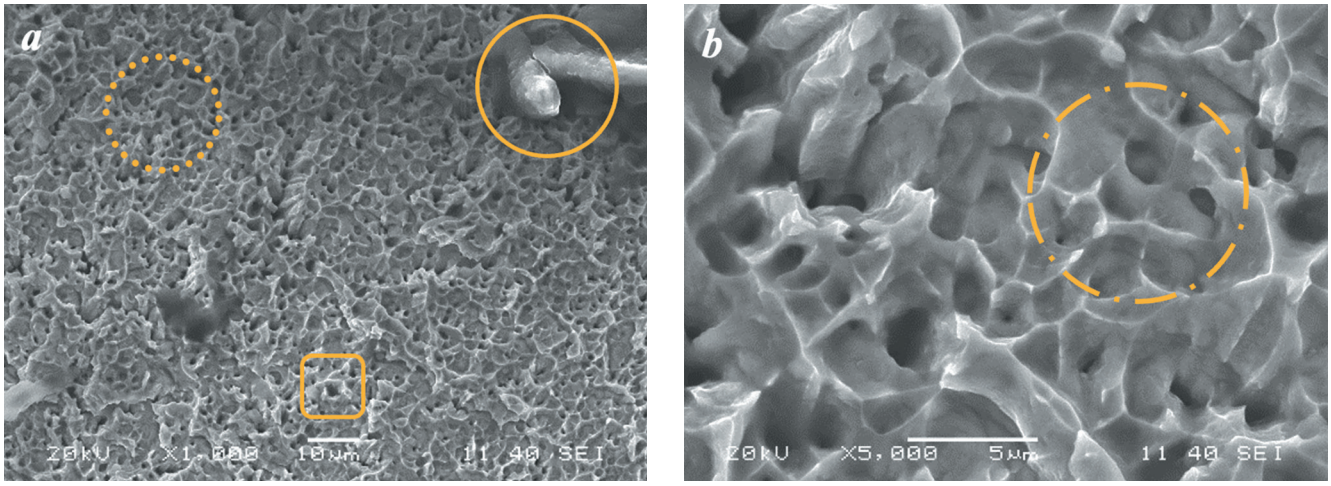

Fig. 6. **Fractograms of the split surface of the loaded, used S-flex 6.25 sample at different magnifications in secondary electrons.**

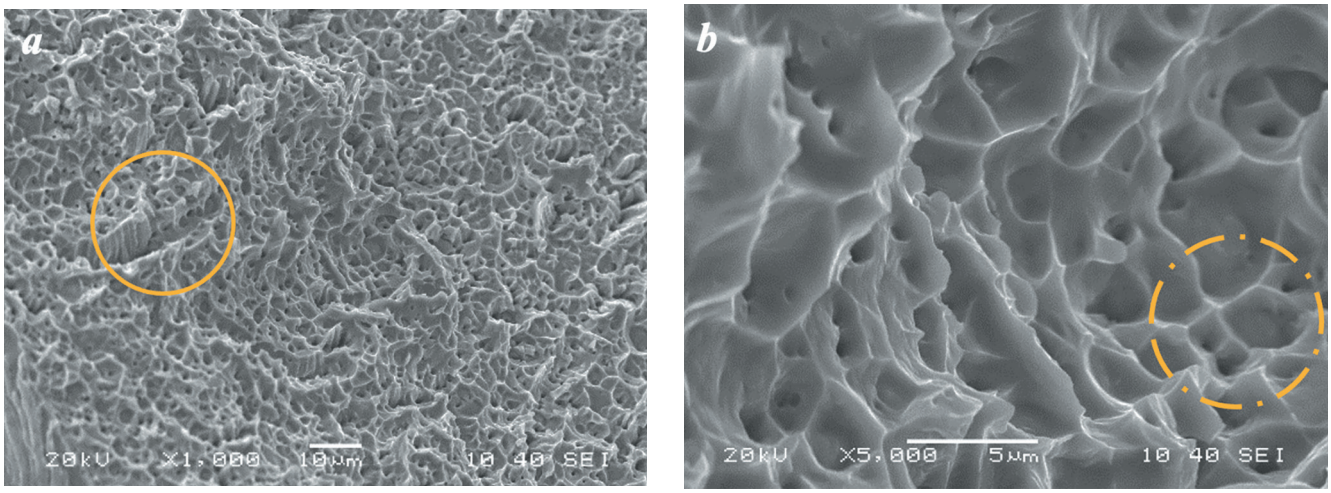

Fig. 7. **Fractograms of the split surface of a new, unused S-flex 4.30 sample at different magnifications in secondary electrons.**

Fractograms of the split surface of the cross-section of the new unused S-flex 6.25 sample show a partially homogeneous, mostly finely dimpled structure with pointed wedge-shaped edges (Fig. 5a doted circle) of structural elements ranging in size from 500 nm to 6.5 microns. Often located pores (Fig. 5a circles) of an isotropic shape are noted in most structural elements of the surface and are evenly distributed over the surface of the sample cleavage. Pores (Fig. 5b circles and dotes) (as on other samples) are observed mainly in the central zones of structural elements in the center of the pits and have sizes from 500 nm to 1.4 microns. Cracks consisting of merged large pores are noted on some areas of the surface.

Fractograms of the split of the cross-section of the S-flex 6.25 sample obtained as a result of a series of workloads (4 cycles), including a twist fracture (volumetric stretching), show a mostly homogeneous, finely dimpled structure with slightly swollen, more flat than on the new sample, wedge-shaped edges of structural elements, sizes from 500 nm to 4.7 microns (Fig. 6a). Often located isotropic pores (Fig. 6a circles and dotes) are also evenly distributed over the sample cleavage surface, are observed mainly in the central zones

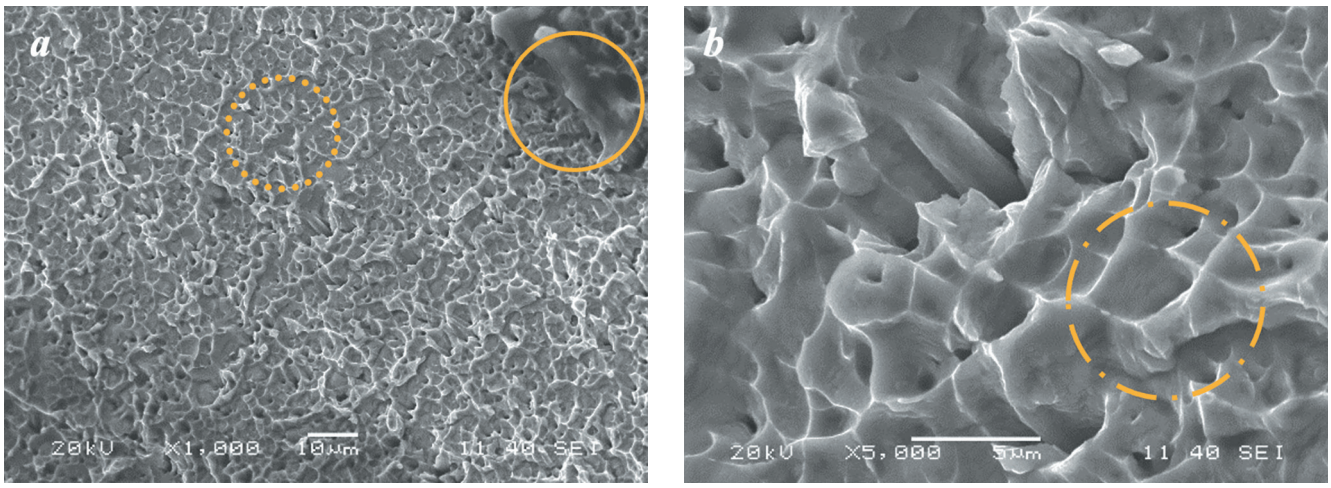

Fig. 8. **Fractograms of the split surface of the loaded, used S-flex 4.30 sample at different magnifications in secondary electrons.**

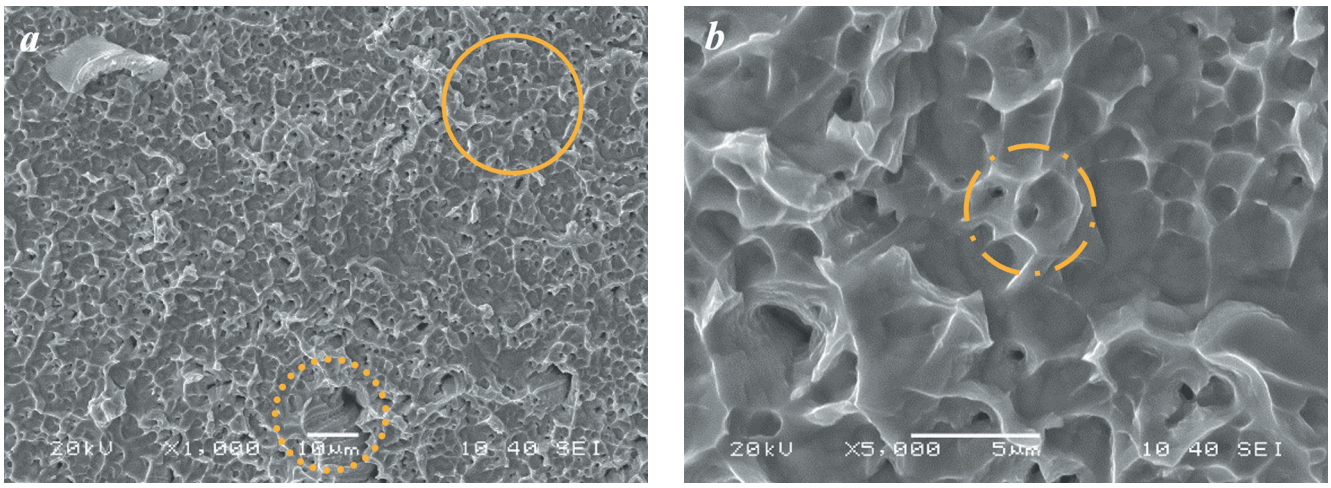

Fig. 9. **Fractograms of the split surface of used S-flex 4.35 sample at different magnifications in secondary electrons.**

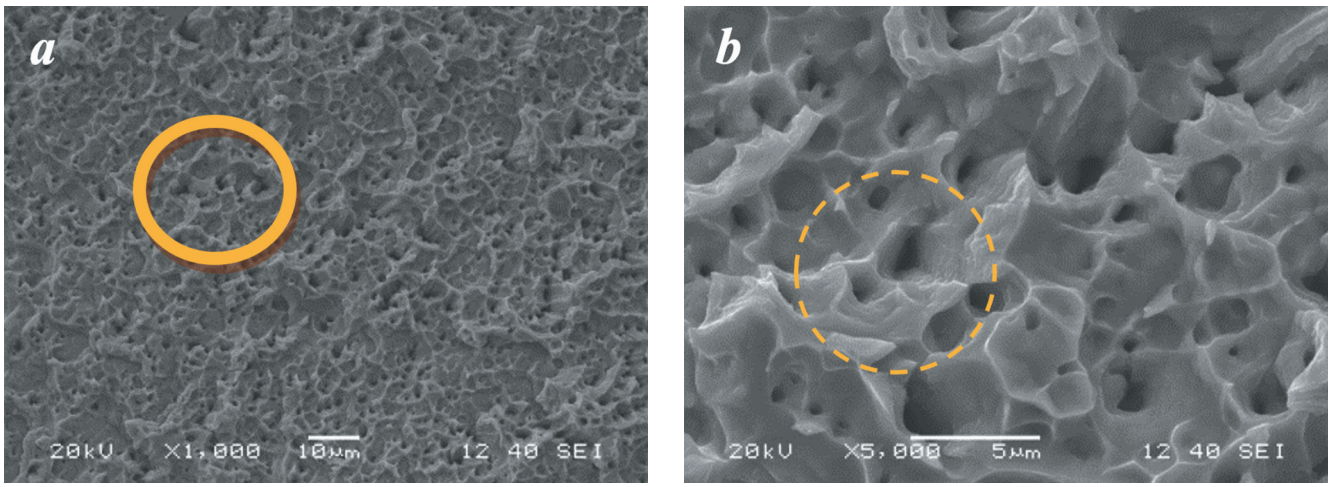

Fig. 10. **Fractograms of the split surface of the loaded, used S-flex 4.35 sample at different magnifications in secondary electrons.**

of most structural elements and have sizes from 300 nm to 1.7 microns. Small conglomerates (Fig. 6a circles) of alloy of various shapes formed during stretching and separation and organic inclusions from the sample surface were found on the rock. Several pores merge with each other and form a small crack.

Fractograms of the split surface of the cross-section of the new unused S-flex 4.30 sample show a homogeneous finely dimpled structure with pointed wedge-shaped edges and cliff-like (Fig. 7a) fragments of structural elements ranging in size from 1 to 6 microns. The images show isotropic pores (Fig. 7b) located in most of the structural elements of the surface and evenly distributed over the surface of the sample cleavage. Pores (Fig. 7b) are observed mainly in the central zones of structural elements in the center of the pits and have sizes from 400 nm to 1 microns. No cracks were found.

Fractograms of the split of the cross-section of the S-flex 4.30 sample obtained as a result of a series of workloads (7 cycles), including a twist fracture (volumetric stretching), also show a homogeneous finely dimpled structure with wedge-shaped edges (Fig. 8a circles) of structural elements oriented in one direction and slightly swollen, ranging in size

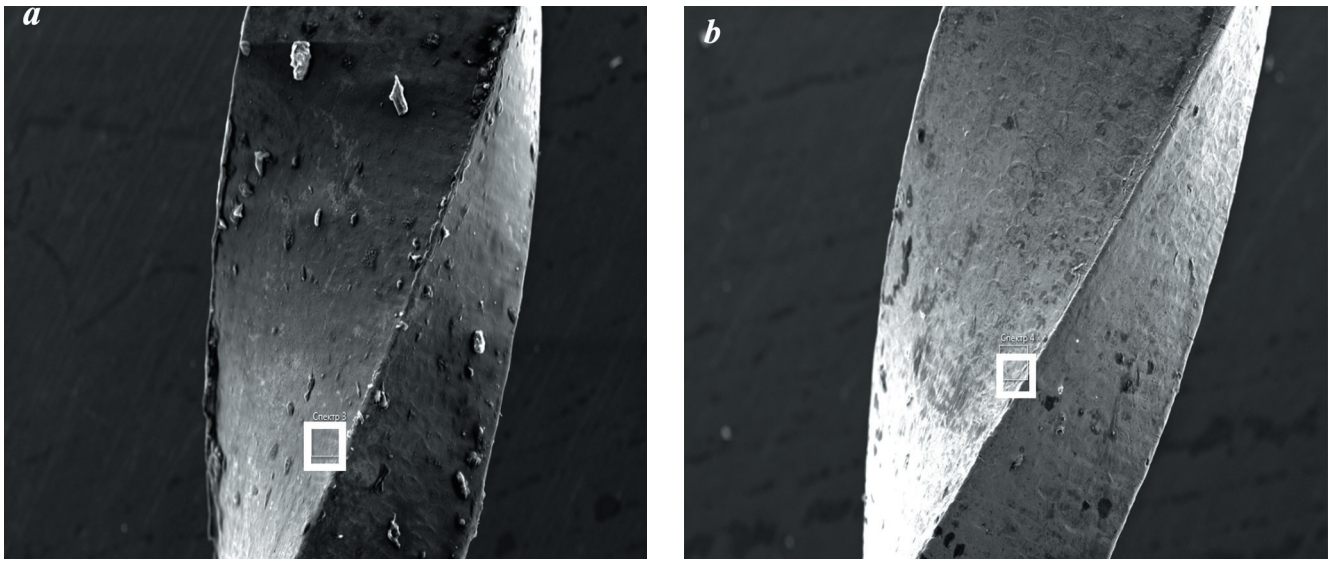

Fig. 11. **Electronic image of sample s-flexi 04/30. The images indicate the areas from which spectra A and B were accumulated.**

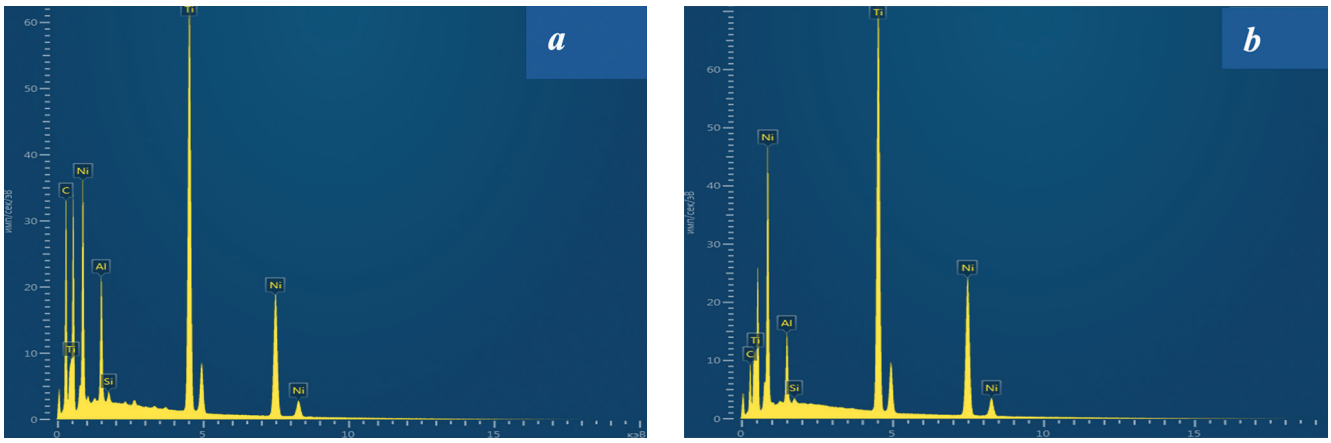

Fig. 12. **Electronic spectrum imaging S-flexi 04/30. The images indicate the areas from which spectra A and B were accumulated.**

from 1 to 7.5 microns. Isotropic pores (Fig. 8a circles and dotes) are observed mainly in the central zones of structural elements and have sizes from 400 nm to 2 microns. The vapors are observed in moderate amounts, in about half of the structural elements and are evenly distributed over the surface of the sample cleavage. Small conglomerates (Fig. 8a circles) of alloy of various shapes formed during stretching and separation and organic inclusions from the sample surface were found on the rock. No cracks were found.

Fractograms of the split surface of the cross-section of the new unused S-flex 4.35 sample show a stepped break with alloy surges and a homogeneous finely dimpled structure, pointed wedge-shaped edges and rock-like fragments (Fig. 9a circles) of structural elements ranging in size from 0.6 microns to 6.5 microns. The images show abundant isotropic pores (Fig. 9b doted circle) located in most of the structural elements of the surface and evenly distributed over the surface of the sample cleavage (Fig. 9 dotes and circles). Pores are observed mainly in the central zones of structural elements in the center of the pits and have a large size spread – from 300 nm to 2.5 microns. Some pairs merge with each other and form small cracks.

Fractograms of the split of the cross-section of the S-flex 4.35 sample obtained as a result of a series of workloads (4 cycles), including a twist fracture (volumetric stretching), show a homogeneous finely dimpled structure (Fig. 9a circles) with slightly swollen wedge-shaped edges of structural elements ranging in size from 0.6 microns to 7.5 microns. Isotropic pores (Fig. 9b doted circles) are observed mainly in the central zones of the structural elements and have sizes as in the new sample from 300 nm to 2.4 microns (Fig. 9). Pores (Fig. 9b doted circles) are present in large numbers and are noted in most structural elements and are also evenly distributed over the surface of the sample cleavage. Small conglomerates of alloy of various shapes were found on the rock (Fig. 9 squares), which appeared during stretching and separation. Some pairs merge with each other and form small cracks.

Fractograms of the split of the cross-section of the S-flex 4.35 sample obtained as a result of a series of workloads (4 cycles), including a twist fracture (volumetric stretching), show a homogeneous finely dimpled structure (Fig. 10a circles) with slightly swollen wedge-shaped edges of structural elements ranging in size from 0.6 microns to 7.5 microns. Isotropic pores (Fig. 10b doted circle) are observed mainly in the central zones of the structural elements and have sizes as in the new sample from 300 nm to 2.4 microns. Pores (Fig. 10b doted circles) are present in large numbers and are noted in most structural elements and are also evenly distributed over the surface of the sample cleavage. Small conglomerates of alloy of various shapes were found on the rock (Fig. 10c), which appeared during stretching and separation. Some pairs merge with each other and form small cracks.

After obtaining a detailed image and a clear difference in structure between the files before and after loading. It was necessary to see whether there would be changes in the composition of the nickel-titanium S-Flexi files after loading (Fig. 11a) and without loading (Fig. 11b)

No changes in the appearance of the surface of the samples before and after loading were detected, one can only notice that after processing the surface looks a little cleaner. The images indicate the areas in which the spectra were accumulated to determine the qualitative and quantitative elemental composition (Fig. 12).

The table 1 shows that sample 1 consists of an alloy of titanium, nickel, aluminum and silicon. After loading, the content of Ti, Ni and Si increases, but the content of oxygen and aluminum decreases.

Table 1. **Quantitative composition**

	O	Al	Si	Ti	Ni
spectrum 1 (at%)	62, 2	6, 02	0, 41	18, 44	12, 92
spectrum 2 (at%)	55, 07	4, 37	22, 5	22, 4	17, 84

DISCUSSION

According to the results of the study of resistance to cyclic loading, showed better results than those results given by the manufacturer and the results of chemical and temperature loading showed high corrosion resistance and absence and preservation of plasticity after temperature loading. At the same time, the lowest indicators were for the S-flexi 04/20 file, but the high indicators were the S-flexi 04/30.

CONCLUSION

High-quality and safe mechanical treatment of root canals is possible when using nickel-titanium S-flexi files.

REFERENCES:

1. Anonymous. ASTM F 2004-17. Standard test method for transformation temperature of nickel-titanium alloys by thermal analysis. Am. Soc. Test. Mater. 2016 doi: 10.1520/F2082_F2082M-16.
2. Cho O.I., Versluis A., Cheung G.S., Ha J.H., Hur B., Kim H.C. Cyclic fatigue resistance tests of Nickel-Titanium rotary files using simulated canal and weight loading conditions. Restor. Dent. Endod. 2013;38:31–35
3. Di Nardo D., Zanza A., Seracchiani M., Donfrancesco O., Gambarini G., Testarelli L. Angle of Insertion and Torsional Resistance of Nickel-Titanium Rotary Instruments. Materials. 2021;14:3744.
4. Gao Y, Shotton V, Wilkinson K, Phillips G, Johnson WB Effects of raw material and rotational speed on the cyclic fatigue of ProFile Vortex rotary instruments. Journal of Endodontics 36, 2010 .1205–9.
5. Gutmann JL, Gao Y Alteration in the inherent metallic and surface properties of nickel-titanium root canal instruments to enhance performance, durability and safety: a focused review. International Endodontic Journal 45, 2012. 113–28.
6. Otsuka K, Ren X Physical metallurgy of Ti-Ni based shape memory alloys. Progress in Materials Science 50, 2005. 511–678.
7. Pedullà E, Grande NM, Plotino G, Pappalardo A, Rapisarda E (2011) Cyclic fatigue resistance of three different nickel-titanium instruments after immersion in sodium hypochlorite. Journal of Endodontics 37, 1139–42.
8. Ha J.H., Kim S.K., Cohenca N., Kim H.C. Effect of R-phase heat treatment on torsional resistance and cyclic fatigue fracture. J. Endod. 2013;39:389–393. doi: 10.1016/j.joen.2012.11.028.
9. Hou X, Yahata Y, Hayashi Y, Ebihara A, Hanawa T, Suda H (2011) Phase transformation behaviour and bending property of twisted nickel-titanium endodontic instruments. International Endodontic Journal 44, 253–8.
10. Kim HC, Yum J, Hur B, Cheung GS Cyclic fatigue and fracture characteristics of ground and twisted nickel-titanium rotary files. Journal of Endodontics 36, 2010. 147–52.
11. Kuhn G, Jordan L Fatigue and mechanical properties of nickel-titanium endodontic instruments. Journal of Endodontics 28, 2002. 716–20.
12. Larsen CM, Watanabe I, Glickman GN, He J (2009) Cyclic fatigue analysis of a new generation of nickel-titanium rotary instruments. Journal of Endodontics 35, 401-3.
13. Loska S., Basiaga M., Pochrząst M., Łukomska-Szymańska M., Walke W., Tyrlik-Held J. Comparative characteristics of endodontic drills. Acta Bioeng Biomech. 2015;17:75–83
14. Martins J.N.R., Silva E.J.N.L., Marques D., Belladonna F., Simões-Carvalho M., Vieira V.T.L., Antunes H.S., Braz Fernandes F.M.B., Versiani M.A. Design, metallurgical features, mechanical performance and canal preparation of six reciprocating instruments. Int. Endod. J. 2021;54:1623–1637. doi: 10.1111/iej.13529.
15. Martín B, Zelada G, Varela P, et al. (2003) Factors influencing the fracture of nickel-titanium rotary instruments. International Endodontic Journal 36, 262–6.
16. Morgental RD, Vier-Pelisser FV, Kopper PM, de Figueiredo JA, Peters OA (2013) Cutting efficiency of conventional and martensitic nickel-titanium instruments for coronal flaring. Journal of Endodontics 39, 1634–8.
17. Pereira E.S.J., Peixoto I.F.C., Viana A.C.D., Oliveira I.I., Gonzalez B.M., Buono V.T.L., Bahia M.G.A. Physical and mechanical properties of a thermomechanically treated NiTi wire used in the manufacture of rotary endodontic instruments. Int. Endod. J. 2012;45:469–474.
18. Pirani C., Iacono F., Generali L., Sassatelli P., Nucci C., Lusvarghi L. HyFlex EDM: Superficial features, metallurgical analysis and fatigue resistance of innovative electro discharge machined NiTi rotary instruments. Int. Endod. J. 2016;49:483–493. doi: 10.1111/iej.12470.
19. Pedullà E, Lo Savio F, Boninelli S, et al. Torsional and cyclic fatigue resistance of a new nickel-titanium instrument manufactured by electrical discharge machining. Journal of Endodontics 42, 2016. 156–9.
20. Pedullà E, Plotino G, Grande NM, Pappalardo A, Rapisarda E (2012) Cyclic fatigue resistance of four nickel-titanium rotary instruments: a comparative study. Annali Di Stomatologia (Roma) 3, 59–63.
21. Thompson SA An overview of nickel-titanium alloys used in dentistry. International Endodontic Journal 33, 2000. 297–310.
22. Tripi TR, Bonaccorso A, Condorelli GG Cyclic fatigue of different nickel-titanium endodontic rotary instruments. Oral Surgery, Oral Medicine, Oral Pathology, Oral Radiology, and Endodontology 102, 2006. e106–14.
23. Shen Y., Zhou H.M., Wang Z., Campbell L., Zheng Y.F., Haapasalo M. Phase transformation behavior and mechanical properties of thermomechanically treated K3XF nickel-titanium instruments. J. Endod. 2013;39:919–923. doi: 10.1016/j.joen.2013.04.004.
24. Ye J, Gao Y Metallurgical characterization of M-Wire nickel-titanium shape memory alloy used for endodontic rotary instruments during low-cycle fatigue. Journal of Endodontics 38, 2012. 105–7.
25. Walia HM, Brantley WA, Gerstein H Initial investigation of bending and torsion properties of nitinol root canal files. Journal of Endodontics, 14, 1988. 346–51.
26. Wycoff RC, Berzins DW An in vitro comparison of torsional stress properties of three different rotary nickel-titanium files with a similar cross-sectional design. Journal of Endodontics 38, 2012. 1118–20.
27. Zhou HM, Shen Y, Zheng W, Li L, Zheng YF, Haapasalo M (2012) Mechanical properties of controlled memory and superelastic nickel-titanium wires used in the manufacture of rotary endodontic instruments. Journal of Endodontics 38, 1535–40.
28. Zhou H, Peng B, Zheng YF An overview of the mechanical properties of nickel-titanium endodontic instruments. Endodontic Topics 29, 2013. 42–54.
29. Zinelis S, Darabara M, Takase T, Ogane K, Papadimitriou GD The effect of thermal treatment on the resistance of nickel-titanium rotary files in cyclic fatigue. Oral Surgery, Oral Medicine, Oral Pathology, Oral Radiology, and Endodontology 103, 2007. 843–7.
30. Zinelis S, Eliades T, Eliades G A metallurgical characterization of ten endodontic Ni-Ti instruments: assessing the clinical relevance of shape memory and superelastic properties of Ni-Ti endodontic instruments. International Endodontic Journal 43, 2010.125–34.

AUTHOR INFORMATION:

Zurab S. Khabadze – Associate Professor of the Department of Therapeutic Dentistry ORCID ID 0000-0002-7257-5503
Farukh R. Ismailov – postgraduate student of the Department of Therapeutic Dentistry

Peoples' Friendship University of Russia" (RUDN University). 6 Miklukho-Maklaya st, Moscow, 117198, Russia

AUTHOR'S CONTRIBUTION:

Zurab S. Khabadze – drafted the article or revised it critically for important intellectual content; approved the version to be published.
Farukh R. Ismailov – the acquisition, analysis, or interpretation of data for the article.

Координаты для связи с авторами / Coordinates for communication with authors:
Farukh R. Ismailov, E-mail: ifarukh@list.ru